Nanoscale Advances

ROYAL SOCIETY OF CHEMISTRY

PAPER

View Article Online
View Journal | View Issue

Cite this: *Nanoscale Adv.*, 2021, **3**, 3491

Identifying the presence of magnetite in an ensemble of iron-oxide nanoparticles: a comparative neutron diffraction study between bulk and nanoscale

D. González-Alonso, †*[a] J. I. Espeso,[a] H. Gavilán,[b] L. J. Zeng,[c] M. T. Fernández-Díaz,[d] G. Subías, [e] I. de Pedro,[a] J. Rodríguez Fernández,[a] P. Bender,‡[a] L. Fernández Barquín[a] and C. Johansson[f]

Received 7th October 2020
Accepted 23rd March 2021

DOI: 10.1039/d0na00830c

rsc.li/nanoscale-advances

Scientific interest in iron-oxides and in particular magnetite has been renewed due to the broad scope of their fascinating properties, which are finding applications in electronics and biomedicine. Specifically, iron oxide nanoparticles (IONPs) are gathering attraction in biomedicine. Their cores are usually constituted by a mixture of maghemite and magnetite phases. In view of this, to fine-tune the properties of an ensemble of IONPs towards their applications, it is essential to enhance mass fabrication processes towards the production of monodisperse IONPs with controlled size, shape, and stoichiometry. We exploit the vacancy sensitivity of the Verwey transition to detect the presence of magnetite. Here we provide direct evidence for the Verwey transition in an ensemble of IONPs through neutron diffraction. This transition is observed as a variation in the Fe magnetic moment at octahedral sites and, in turn, gives rise to a change of the net magnetic moment. Finally, we show this variation as the microscopic ingredient driving the characteristic kink that hallmarks the Verwey transition in thermal variation of magnetization.

Introduction

Magnetite is an ancient magnetic material that is nowadays intensively studied due to its widespread applications in different fields, such as in oxide electronics,[1] biomedicine,[2] solid-state energy conversion devices,[3] non-volatile resistive switching,[4] and gate voltage induced phase transition,[5] among others. Moreover, recent biomedical applications involve the use of iron oxide nanoparticles (IONPs), mainly as contrast agents,[6] in hyperthermia treatments,[2,7] and as magnetic carriers.[8] Precisely, magnetite is the desirable iron-oxide phase to form nanoparticle cores due to its high saturation magnetization values.[2,9,10] At room temperature, magnetite (Fe_3O_4) crystallizes in an inverse-spinel cubic structure, *i.e.*, AB_2O_4, with a space group $Fd\bar{3}m$ and a lattice parameter $a \approx 8.39$ Å.[11] This is formally written as $Fe^{3+}_A[Fe^{2+}Fe^{3+}]_BO_4$, with two types of Fe-atoms. A-sites are occupied by tetrahedrally coordinated Fe^{3+} cations, whereas B-sites are occupied by both Fe^{2+} and Fe^{3+} cations.

Pioneering studies noticed the existence of a low-temperature transition in magnetite by means of specific heat,[12] magnetization,[13] and electrical resistivity[14] measurements. It was only after the influential study conducted in 1939 by Verwey[15] that the transition was interpreted in detail from the observation of two concurrent effects in a polycrystalline magnetite sample. Briefly, upon cooling, an abrupt decrease in DC-conductivity of 2 orders of magnitude at around $T_V \approx 117$ K (metal–insulator transition MIT) was found. This was accompanied by a crystallographic symmetry reduction from its high-temperature (cubic) phase. The advent of high-resolution X-ray synchrotron instrumentation has allowed establishing the structural origin of the Verwey transition.[16–18] In addition, the anisotropy increases[19] because of the gradual change in the magnetic easy-axis from the low-temperature monoclinic phase [001] to the cubic [111] one.[20–22] In this sense, a recent study confirms magnetic order fluctuations as the underlying origin of the Verwey transition.[23] In contrast to X-ray diffraction that provides atomic structure information (*e.g.*, lattice parameters,

[a]*Department CITIMAC, Faculty of Science, University of Cantabria, 39005, Santander, Spain. E-mail: galonsod@unican.es*
[b]*Instituto de Ciencia de Materiales de Madrid, ICMM/CSIC, 28049, Madrid, Spain*
[c]*Department of Physics, Chalmers University of Technology, 41296, Göteborg, Sweden*
[d]*Institut Laue-Langevin, 38042, Grenoble, France*
[e]*Instituto de Ciencia de Materiales de Aragón, Departamento de Física de la Materia Condensada, CSIC-Universidad de Zaragoza, 50009, Zaragoza, Spain*
[f]*RISE Research Institutes of Sweden, 411 33, Göteborg, Sweden*
† Present address: Department of Physics, Campus de Viesques, University of Oviedo, 33203, Gijón, Spain.
‡ Present address: Heinz Maier-Leibnitz Zentrum (MLZ), Technische Universität München, D-85748, Garching, Germany.

crystal structure, and atomic species), neutron diffraction additionally provides information on the magnetic structure (*e.g.*, atomic magnetic moment). Combining both atomic and magnetic structural information, neutron diffraction is crucial in the understanding of magnetic crystalline materials.

In this study, we present a detailed investigation focused on the thermal evolution of the magnetic moment in an ensemble of IONPs, using polycrystalline magnetite for comparison. It should be kept in mind that nominal samples of magnetite might be affected by a certain quantity of maghemite (γ-Fe_2O_3). In this sense, the evaluation of the coexistence of magnetite and maghemite phases has recently been tackled, and it was demonstrated that the magnetite powder sample under investigation here presents 98(1)% magnetite purity.[24] Finally, we reveal the Verwey transition by means of a kink in the thermal variation of the magnetic moment at the octahedral Fe_B-sites obtained by neutron powder diffraction (NPD) analysis.

Experimental

The polycrystalline magnetite Fe_3O_4 powder sample was provided by the Department of Physics at the Technical University of Denmark. The ensemble of IONPs was produced by an oxidative precipitation method reported in ref. [25] and [26] and subsequently coated with dextran *via* a high-pressure homogenization procedure. Eventually, the IONPs were magnetically fractionated to reduce size inhomogeneities.[26] Transmission electron microscopy (TEM) and high-resolution transmission electron microscopy (HRTEM) were carried out on an FEI Tecnai G2 T20 (equipped with an LaB_6 electron gun) and an FEI Titan 80-300, respectively. For subsequent characterization of the IONP ensemble, droplets of water-dispersed IONPs were placed on a carbon-coated copper grid. AC-susceptibility was assessed by using a Quantum Design MPMS-system at a frequency of 0.5 Hz with a field amplitude of $\mu_0 H_{ac} \approx 0.3$ mT. NPD experiments were carried out using a liquid helium cryostat on a high-flux two-axis diffractometer D1B at the Institute Laue–Langevin (Grenoble, France).[27] The sample was loaded into a cylindrical vanadium container and data were collected at selected temperatures between 5 and 300 K. Each diffraction pattern was measured with an acquisition time of 0.5 hours within the 2θ range ~15–128° in steps of $\Delta 2\theta = 0.1°$ and with a wavelength of $\lambda \cong 2.52$ Å. The Rietveld refinement analysis of neutron diffraction data was performed using the FULLPROF software[28] with a Thompson–Cox–Hastings pseudo-Voigt profile function to describe the shape of the diffraction peaks. This method allows a simultaneous evaluation of the crystalline and magnetic structure through the variation of fitting parameters such as the lattice parameter, the scale factor, and the value of the magnetic moment, among others. The quality of the fit could be evaluated *via* the Bragg (R_{Bragg}) and magnetic Bragg (R_{mag}) factors, which are the two more reliable agreement-factors to ascertain a Rietveld analysis. Values below 20% are acceptable, especially for an ensemble of nanoparticles. The temperature dependence of the DC-magnetization $M(T)$ was recorded at several magnetic fields $\mu_0 H = 1$, 3 and 5 T in the temperature range $5 \leq T \leq 300$ K using a Quantum Design PPMS magnetometer.

Results and discussion

Fig. 1 shows a representative TEM image of the ensemble of IONPs in which nanoparticles are grouped, forming agglomerates of different sizes. The ensemble is constituted by nearly monodisperse single-cores of cuboid shape (see the upper left inset in Fig. 1). As observed in the log-normal size-distribution displayed in the upper right inset, the ensemble presents a number-weighted mean value of $D = 28$ nm and a standard deviation of 4 nm. TEM and XRD analyses of the cuboid-shaped IONPs agree in terms of the average particle size, as discussed elsewhere.[29] According to Fock and Bogart *et al.*[24] and with the aid of the room-temperature Mössbauer spectrum the amount of magnetite was estimated to be 28(10) wt.%, *i.e.*, 72 wt.% of maghemite, which confirms the coexistence of magnetite and maghemite phases in the ensemble of IONPs.[29]

Fig. 2 depicts the real $\chi'(T)$ and complex $\chi''(T)$ contributions to the AC-susceptibility for bulk magnetite[24] and the ensemble of IONPs. At low-temperatures (below 50 K), a kink in $\chi'(T)$ and a broad peak in $\chi''(T)$ are observed for both samples. The origin of this low-temperature anomaly still remains unclear.[30–32] It is worth noting that there is a clear jump in $\chi'(T)$ at around 120 K for bulk magnetite , whereas no sign of such magnetic behavior is observed for the IONPs.[33] On the other hand, the $\chi''(T)$ complex contribution to the AC-susceptibility (red empty triangles) reveals a clear peak for bulk magnetite, that is barely observed in the ensemble. To make this peak clearly visible, we have subtracted the black solid line appearing at the bottom of Fig. 2 (see the resulting peak in red in the right inset of Fig. 2). In the insets of Fig. 2, the integral of $\chi''(T)$ has been represented by blue empty squares to highlight the magnetic correlations for both bulk magnetite and IONP samples. Furthermore, the Verwey transition is only characteristic of highly stoichiometric

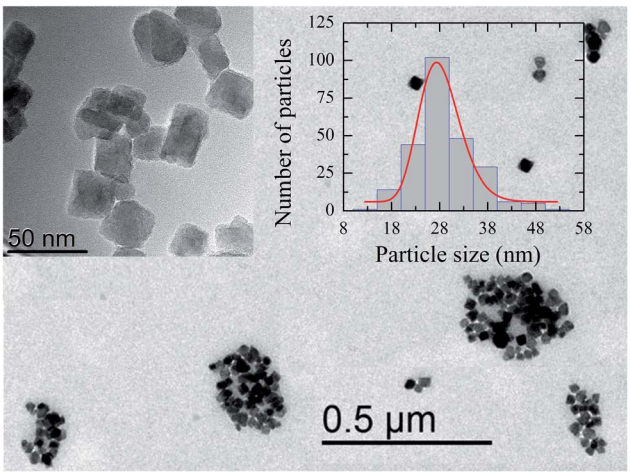

Fig. 1 TEM image of the ensemble of IONPs. The upper left inset shows an HRTEM image of single-core IONPs with a cuboid shape. The log-normal size-distribution of IONPs is displayed in the upper right inset with a number-weighted mean value of 28(4) nm.

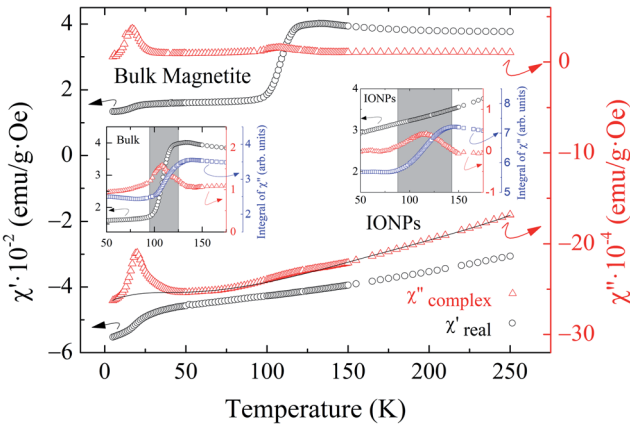

Fig. 2 Temperature evolution of the real $\chi'(T)$ (black open circles) and complex $\chi''(T)$ (red open triangles) contributions to the AC-susceptibility at a frequency of 0.5 Hz for bulk magnetite Fe_3O_4 and IONPs. IONP AC-susceptibility data are vertically shifted for clarity. The insets show the magnification of the AC-susceptibility hallmarking a small broad peak at around 120 K for both samples. In the right inset, $\chi''(T)$ is plotted after subtracting the solid black line, for clarity. Blue open squares depict the integral of $\chi''(T)$ as an indicator of the Verwey transition. Shaded regions delimit the temperature window within which the Verwey transition is expected to occur.

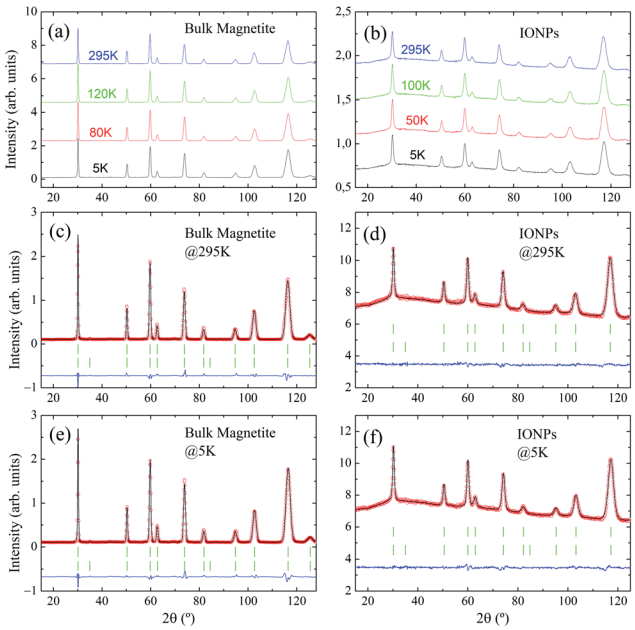

Fig. 3 Representative NPD measurements collected on a D1B for (a, c, e) bulk magnetite and (b, d, f) IONP samples. The patterns are vertically shifted for clarity. Rietveld refinements of the data collected at 295 K and 5 K for (c, e) bulk magnetite and (d, f) IONP samples, respectively. Observed and calculated data are represented by red empty circles and by a solid black line, respectively. Bragg reflections are represented by vertical green bars. The blue line at the bottom corresponds to the observed–calculated difference.

magnetite samples.[34,35] In view of this, we take these broad peaks in both samples as an indicator of the magnetic correlations that are considered in the origin of the Verwey transition.[23,33,36] Therefore, we can confirm that the cores of our ensemble of IONPs are constituted by a mixture of maghemite and magnetite phases.

Representative NPD patterns collected at selected temperatures well below and above the expected Verwey transition temperature ($T_V \approx 120$ K[33,34]) are displayed in Fig. 3(a and b) for bulk magnetite and IONP samples, respectively. As expected, when we draw a comparison between NPD measurements of bulk magnetite and IONPs, a reduction in peak intensity is observed, together with peak broadening. This is a consequence of the nanoscale size of the IONP sample (*ca.* 28 nm). In addition, a small bump in the background of the IONP patterns in the 2θ-range $20° \leq 2\theta \leq 110°$ is also evident. We surmise that this contribution to the background basically originates from the minor scattering of the coating.

Regarding the low-temperature Rietveld refinements displayed in Fig. 3(e and f), no evidence of satellite peaks stemming from the monoclinic $C2/c$ space group was observed.[17] Consequently, the resolution of the instrument D1B does not allow for the recognition of the monoclinic distortions through the Verwey transition. Therefore, to extract quantitative parameters, we are bound to propose a simplified approach in which the high-temperature cubic $Fd\bar{3}m$ will be maintained across the whole temperature range. Thus, in this approach the aim is to procure some parameters which may be connected to the Verwey transition and magnetite content. The cubic structure is valid for both maghemite and magnetite phases.[37] Following this approach, every single peak of the set of NPD patterns taken at different temperatures is indexed (R_B <4%) to the cubic $Fd\bar{3}m$ space group (see Table 1 for crystallographic details). Moreover, an accurate match in the intensities of the peaks is obtained as exemplified by the small residual obtained in the Rietveld analysis (see Fig. 3(c–f)).

Fig. 4(a and b) show the relevant structural changes that occur during the Verwey transition (shaded region), which were

Table 1 Crystallographic information data. Crystal data structure of the cubic $Fd\bar{3}m$ space group, together with a list of standard quality parameters, *i.e.*, goodness of fit χ^2 and agreement factors R_P, R_{WP}, R_{Bragg}, R_{mag}, obtained from the Rietveld analysis at selected temperatures and represented in Fig. 3. The oxygen coordinate parameter u is almost constant (ideally equal to 1/4 (ref. 11))

Atom	Wyckoff position	x	y	z
O	32e	u	u	u
Fe oct	16d	1/2	1/2	1/2
Fe tet	8a	1/8	1/8	1/8

	Bulk magnetite		IONPs	
Parameters	5 K	295 K	5 K	295 K
R_p (%)	3.74	3.39	14.6	13.4
R_{wp} (%)	5.06	4.77	8.48	7.77
R_{Bragg} (%)	2.29	2.63	2.52	3.23
R_{mag} (%)	4.56	4.33	10.0	5.26
χ^2	55.6	45.1	3.55	2.89

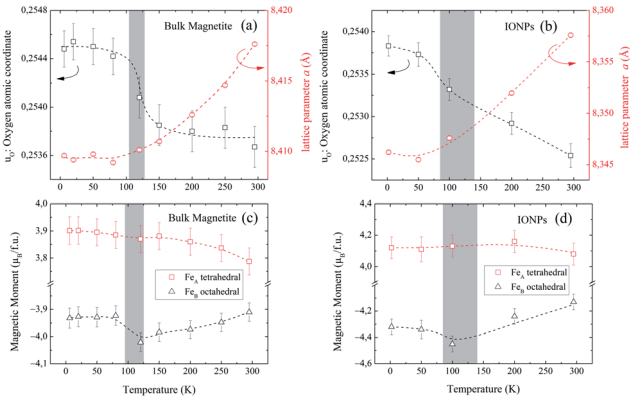

Fig. 4 Results of the Rietveld analysis. Temperature-dependence of the lattice parameter and oxygen atomic coordinate for (a) bulk magnetite and (b) IONP samples. Thermal evolution of the $Fe_{A,B}$-moments for (c) bulk magnetite and (d) IONPs. Shaded regions delimit the temperature-window within which the Verwey transition is expected to occur. Dashed lines are guides to the eye.

obtained in the refinement of bulk magnetite and IONP samples, respectively. For both samples (see Fig. 4(a and b)), the lattice parameters and consequently the volume of the unit cell experience a monotonous increase as the temperature rises above the transition. In contrast, they remain roughly constant below the Verwey transition temperature. The variation in the temperature evolution of the a lattice parameter is accompanied by the change in the oxygen coordinate u (see Fig. 4(a and b)). This shrinkage of u across the transition relates to the structural change. Precisely, this marks a first-order phase transition from the low-temperature phase to the high-temperature cubic phase in magnetite[38,39] (see Fig. 4). The refined values of u agree with those reported in the literature,[40,41] despite being slightly larger than those in the case of cubic closest-packing, $u = 0.25$.[41] In fact, the oxygen-coordinate u is closely related to the Fe_i-O bond-lengths as shown in the following expressions:[42]

$$d_{Fe_B-O} = a(1/2 - u) \quad (1)$$

$$d_{Fe_A-O} = \sqrt{3}a(u - 1/8) \quad (2)$$

Magnetic Rietveld refinements were performed using a ferrimagnetic structure for all temperatures (see Fig. 3(c–f) and the agreement factors compiled in Table 1). The thermal evolution of the magnetic moments obtained from neutron diffraction is depicted in Fig. 4(c and d). Interestingly, a small kink at the octahedral sites for both samples is observed in the vicinity of the Verwey transition. We surmise that this feature is related to the kink depicted by bulk magnetite in the real contribution to the AC-susceptibility but does not appear for IONPs (see Fig. 2). In addition, it is reasonable to expect that the trivalent Fe (A- and B-) sites are mutually compensated, which in turn suggests that Fe_B^{2+} cations at octahedral-sites are the ones contributing to the net magnetization value, therefore, corroborating the ferrimagnetic coupling between A and B sublattices, while Fe-sites of the same sublattice (A or B) are ferromagnetically coupled. It is worth reminding here that tetrahedral moments halve the multiplicity of B-sites (see Table 1). Such ferrimagnetic behavior is depicted in more detail in Fig. 5(a and b) through the inspection of the thermal evolution of the Fe magnetic moments. A general trend of the values for both A- and B-sites to decrease with increasing temperature towards T_C ($T_C \approx 850$ K for bulk magnetite[24]) is noticed. Although the magnitudes of the Fe moments are rather similar for both sites, Fig. 5(a and b), they reveal a clear change at the octahedral sites for both samples. Thus, our Rietveld refinements provide clear evidence for the change in magnetic moments exhibited at the octahedral sites in our samples across the Verwey transition. Specifically, this positive variation in the octahedral moment of 0.09(5) $\mu_B/f.u.$ appearing in the bulk magnetite sample agrees well with that reported by magnetic circular dichroism studies of Fe^{2+} thin films.[43,44] Furthermore, though no trace of the Verwey transition is ascertained through $\chi'(T)$ or $M(T)$ for the IONP sample, neutron diffraction reveals the local magnetic order at the Fe octahedral sites. We suggest that this masked Verwey transition is due to the texture effects of the IONPs.

According to Hund's rules, magnetite has a spin moment per formula unit (f.u.) of 4.0 μ_B, where the ground state of Fe^{3+} cations ($3d^5$, $6S_{5/2}$) corresponds to $\mu_{Fe^{3+}} = \mu_B g_S S = 5\ \mu_B$ (with $g_S = 2$ and $S = 5/2$), and for Fe^{2+} ($3d^6$, $5D_4$), it is $\mu_{Fe^{2+}} = \mu_B g_S S = 4\ \mu_B$ ($g_S = 2$ and $S = 2$). To complete our analysis, we performed a quantitative reconstruction of the *net magnetic moment* (per f.u.) by using the refined magnetic moments as described in the following formula:

$$\mu_{net} = 2\mu^{Fe_B}Occ^{Fe_B} - \mu^{Fe_A}Occ^{Fe_A} \quad (3)$$

where $\mu^{Fe\text{-}i}$ and $Occ^{Fe\text{-}i}$ are the $Fe_{A,\ B}$ magnetic moment and the occupancy of the $Fe_{A,\ B}$-site, respectively. The thermal evolution of the *net magnetic moment* is depicted in Fig. 5(c and d) for both

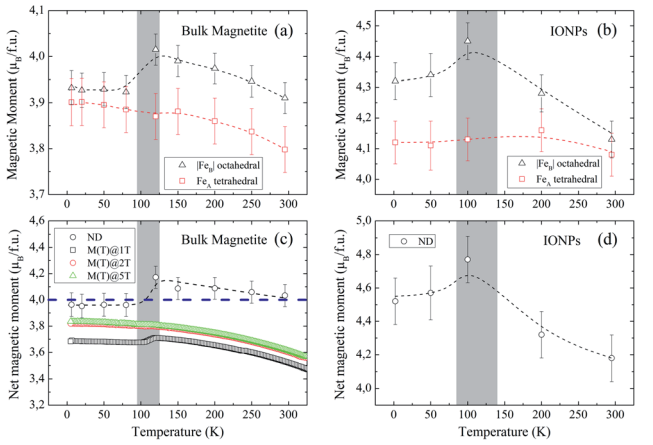

Fig. 5 Thermal variation of the $Fe_{A,\ B}$ magnetic moment for (a) bulk magnetite and (b) IONP samples. Thermal evolution of the net magnetic moment per formula unit (f.u.) for (c) bulk magnetite and (d) IONPs. The blue dashed line corresponds to the theoretical net moment value for stoichiometric magnetite. Dashed lines are guides to the eye.

samples. For the bulk magnetite sample, we also compared the macroscopic $M(T)$ curves at different magnetic fields to the one obtained from refinement, as seen in Fig. 5(c). Due to the impossibility of extracting the real amount of coating from IONPs, we refused to attempt the same estimation for the IONPs. The reconstructed moment (ND without a magnetic field) lies within the theoretical value (dashed blue line in Fig. 5(c)) reported in the literature for magnetite.[45] As expected, at high enough fields, *i.e.*, $\mu_0 H = 3$ & 5 T, the eventual (macroscopic) kink vanishes. From its visual inspection, the reconstructed moment is correlated with the kink of the bulk magnetite sample across the Verwey transition (see AC and DC measurements displayed in Fig. 2 and 5(c), respectively). This in turn is directly related to the variation in the octahedral moment (shown in Fig. 4(c and d) and 5(a and b)) and gives rise to a change in the net magnetic moment of 0.2(1) μ_B/*f.u.* In short, this change perfectly matches with that anticipated by Iizumi *et al.*[11] and is revealed here as the microscopic ingredient driving the characteristic magnetization kink that hallmarks the Verwey transition.

Conclusions

In this work, we have demonstrated that the cores of our ensemble of IONPs comprise maghemite and magnetite phases. TEM measurements show that the IONPs are *ca.* 28 nm in average particle size. A detailed investigation has been performed to trace the masked Verwey transition in the IONP sample, using a bulk magnetite sample for comparison. No indication of the Verwey transition was observed in the real contribution to the AC-susceptibility for the IONP sample, whereas a small broad peak is perceived as an indicator of the transition at *ca.* 120 K in the complex contribution. Neutron diffraction experiments show structural and magnetic changes across the transition. Specifically, the variation of the magnetic moment at the Fe octahedral sites hallmarks the Verwey transition. This microscopic feature matches the kink in both macroscopic $\chi'(T)$ and reconstructed net $M(T)$ for bulk magnetite. Though the local magnetic order is revealed by neutron diffraction, we suggest that the lack of any magnetic trace in $\chi'(T)$ and $M(T)$ is due to texture effects in the IONP sample. We can conclude that our approach has identified key crystallographic parameters to monitor the Verwey transition (*e.g.*, oxygen coordinate parameter u and magnetic moment Fe_B) that can be used as order parameters to trace the transition. The procedure put forward here may open new routes to fine-tune their applications by enhancing the stoichiometry of the ensemble of IONPs.

Author contributions

Conceptualization, D. G.-A.; methodology, L. F. B. and D. G.-A.; formal analysis, J. I. E. and D. G.-A.; investigation, H. G., L. Z., M. T. F. D., I. d. P., J. R. F., P. B. and D. G.-A.; resources, L. F. B. and C. J.; writing–original draft preparation, D. G.-A.; writing–review and editing, J. I. E., G. S., I. d. P., J. R. F., P. B., L. F. B. and D. G.-A. All the authors have read and agreed to the published version of the manuscript.

Conflicts of interest

There are no conflicts to declare.

Acknowledgements

This work has received funding from EU FP7 604448 (NanoMag) and MAT2017-83631-C3-R. The Institute Laue-Langevin is acknowledged for provision of beamtime on the D1B instrument. We thank Dr Oscar Fabelo for his initial guidance in the Rietveld analysis. Dr Lorena González-Legarreta is acknowledged for her critical review and support during the preparation of this manuscript.

References

1 S. de Jong, R. Kukreja, C. Trabant, N. Pontius, C. F. Chang, T. Kachel, M. Beye, F. Sorgenfrei, C. H. Back, B. Bräuer, W. F. Schlotter, J. J. Turner, O. Krupin, M. Doehler, D. Zhu, M. A. Hossain, A. O. Scherz, D. Fausti, F. Novelli, M. Esposito, W. S. Lee, Y. D. Chuang, D. H. Lu, R. G. Moore, M. Yi, M. Trigo, P. Kirchmann, L. Pathey, M. S. Golden, M. Buchholz, P. Metcalf, F. Parmigiani, W. Wurth, A. Föhlisch, C. Schüßler-Langeheine and H. A. Dürr, *Nat. Mater.*, 2013, **12**, 882.

2 B. Pelaz, C. Alexiou, R. A. Alvarez-Puebla, F. Alves, A. M. Andrews, S. Ashraf, L. P. Balogh, L. Ballerini, A. Bestetti, C. Brendel, S. Bosi, M. Carril, W. C. W. Chan, C. Chen, X. Chen, X. Chen, Z. Cheng, D. Cui, J. Du, C. Dullin, A. Escudero, N. Feliu, M. Gao, M. George, Y. Gogotsi, A. Grünweller, Z. Gu, N. J. Halas, N. Hampp, R. K. Hartmann, M. C. Hersam, P. Hunziker, J. Jian, X. Jiang, P. Jungebluth, P. Kadhiresan, K. Kataoka, A. Khademhosseini, J. Kopeček, N. A. Kotov, H. F. Krug, D. S. Lee, C.-M. Lehr, K. W. Leong, X.-J. Liang, M. L. Lim, L. M. Liz-Marzán, X. Ma, P. Macchiarini, H. Meng, H. Möhwald, P. Mulvaney, A. E. Nel, S. Nie, P. Nordlander, T. Okano, J. Oliveira, T. H. Park, R. M. Penner, M. Prato, V. Puntes, V. M. Rotello, A. Samarakoon, R. E. Schaak, Y. Shen, S. Sjöqvist, A. G. Skirtach, M. G. Soliman, M. M. Stevens, H.-W. Sung, B. Z. Tang, R. Tietze, B. N. Udugama, J. S. VanEpps, T. Weil, P. S. Weiss, I. Willner, Y. Wu, L. Yang, Z. Yue, Q. Zhang, Q. Zhang, X.-E. Zhang, Y. Zhao, X. Zhou and W. J. Parak, *ACS Nano*, 2017, **11**, 2313.

3 R. Ramos, T. Kikkawa, K. Uchida, H. Adachi, I. Lucas, M. H. Aguirre, P. Algarabel, L. Morellón, S. Maekawa, E. Saitoh and M. R. Ibarra, *Appl. Phys. Lett.*, 2013, **102**, 072413.

4 M. Liu, J. Hoffman, J. Wang, J. Zhang, B. Nelson-Cheeseman and A. Bhattacharya, *Sci. Rep.*, 2013, **3**, 1876.

5 J. Gooth, R. Zierold, J. G. Gluschke, T. Boehnert, S. Edinger, S. Barth and K. Nielsch, *Appl. Phys. Lett.*, 2013, **102**, 073112.

6 J. Pellico, J. Ruiz-Cabello, I. Fernandez-Barahona, L. Gutierrez, A. V. Lechuga-Vieco, J. A. Enríquez, M. Puerto Morales and F. Herranz, *Langmuir*, 2017, **33**, 10239.
7 W. Wu, Z. Wu, T. Yu, C. Jiang and W.-S. Kim, *Sci. Technol. Adv. Mater.*, 2015, **16**, 023501.
8 S. Carregal-Romero, P. Guardia, X. Yu, R. Hartmann, T. Pellegrino and W. J. Parak, *Nanoscale*, 2015, **7**, 570.
9 Q. A. Pankhurst, J. Connolly, S. K. Jones and J. Dobson, *J. Phys. D: Appl. Phys.*, 2003, **36**, R167.
10 F. Ludwig, O. Kazakova, L. Fernández Barquín, A. Fornara, L. Trahms, U. Steinhoff, P. Svedlindh, E. Wetterskog, Q. A. Pankhurst, P. Southern, M. Puerto Morales, M. F. Hansen, C. Frandsen, E. Olsson, S. Gustafsson, N. Gehrke, K. Lüdtke-Buzug, C. Grüttner, C. Jonasson and C. Johansson, *IEEE Trans. Magn.*, 2014, **50**, 5300204.
11 M. Iizumi, T. F. Koetzle, G. Shirane, S. Chikazumi, M. Matsui and S. Todo, *Acta Crystallogr., Sect. B: Struct. Crystallogr. Cryst. Chem.*, 1982, **38**, 2121.
12 R. W. Millar, *J. Am. Chem. Soc.*, 1929, **51**, 215.
13 P. Weiss and R. Forrer, *Ann. Phys.*, 1929, **12**, 279.
14 T. Okamura, *Sci. Rep. Tohoku Imp. Univ.*, 1932, **21**, 231.
15 E. J. Verwey, *Nature*, 1939, **144**, 327.
16 J. P. Wright, J. P. Attflied and P. G. Radaelli, *Phys. Rev. Lett.*, 2001, **87**, 266401.
17 J. Blasco, J. García and G. Subías, *Phys. Rev. B*, 2011, **83**, 104105.
18 M. S. Senn, J. P. Wright and J. P. Attfield, *Nature*, 2012, **481**, 173.
19 R. Reznicek, V. Chlan, H. Stepankova, P. Novak and M. Marysko, *J. Phys.: Condens. Matter*, 2012, **24**, 055501.
20 J. García, G. Subías, J. Herrero-Martín, J. Blasco, V. Cuartero, M. Concepción Sánchez, C. Mazzoli and F. Yakhou, *Phys. Rev. Lett.*, 2009, **102**, 176405.
21 E. Lima Jr, A. L. Brandl, A. D. Arelaro and G. F. Goya, *J. Appl. Phys.*, 2006, **99**, 083908.
22 R. Aragón, *Phys. Rev. B*, 1992, **46**, 5334.
23 G. Perversi, E. Pachoud, J. Cumby, J. M. Hudspeth, J. P. Wright, S. A. J. Kimber and J. P. Attfield, *Nat. Commun.*, 2019, **10**, 2857.
24 J. Fock, L. K. Bogart, D. González-Alonso, J. I. Espeso, M. F. Hansen, M. Varón, C. Frandsen and Q. A. Pankhurst, *J. Phys. D: Appl. Phys.*, 2017, **50**, 265005.
25 M. Andrés Vergés, R. Costo, A. G. Roca, J. F. Marco, G. F. Goya, C. J. Serna and M. P. Morales, *J. Phys. D: Appl. Phys.*, 2008, **41**, 134003.
26 C. Grüttner, K. Müller, J. Teller, F. Westphal, A. Foreman and R. Ivkov, *J. Magn. Magn. Mater.*, 2007, **311**, 181.
27 D. Alba Venero, P. Bender, J. I. Espeso, L. Fernández Barquín, M. T. Fernández Díaz, D. González-Alonso and Q. A. Pankhurst, *Defining key structural and magnetic parameters for standardising magnetic Fe-oxide nanoparticles for biomedical applications*, Institut Laue-Langevin (ILL), Grenoble, France, 2015.
28 J. Rodríguez-Carvajal, *Newsletter in Commission on Powder Diffraction (IUCr)*, 2001, **26**, 12.
29 D. González-Alonso, J. González, H. Gavilán, J. Fock, L. Zeng, K. Witte, P. Bender, L. Fernández Barquín and C. Johansson, *RSC Adv.*, 2021, **11**, 390.
30 Z. Svindrych, Z. Janu, A. Kozlowski and J. M. Honig, *Phys. Rev. B*, 2012, **86**, 214406.
31 M. Alexe, M. Ziese, D. Hesse, P. Esquinazi, K. Yamauchi, T. Fukushima, S. Picozzi and U. Gösele, *Adv. Mater.*, 2009, **21**, 4452.
32 S. F. Alvarado, W. Eib, F. Meier, D. T. Pierce, K. Sattler, H. C. Siegmann and J. P. Remeika, *Phys. Rev. Lett.*, 1975, **34**, 319.
33 F. J. Walz, *J. Phys.: Condens. Matter*, 2002, **14**, R285.
34 J. M. Honig, *J. Alloys Compd.*, 1995, **229**, 24.
35 J. B. Yang, X. D. Zhou, W. Yelon, W. J. James, Q. Cai, K. Gopalakrishnan, S. K. Malik, X. C. Sun and D. E. Nikles, *J. Appl. Phys.*, 2004, **95**, 7540.
36 L. V. Gasparov, A. Rush, G. Güntherodt and H. Berger, *Phys. Rev. B*, 2009, **79**, 144303.
37 C. Pecharromán, T. González-Carreño and J. E. Iglesias, *Phys. Chem. Miner.*, 1995, **22**, 21.
38 G. K. Rozenberg, M. P. Pasternak, W. M. Xu, Y. Amiel, M. Hanfland, M. Amboage, R. D. Taylor and R. Jeanloz, *Phys. Rev. Lett.*, 2006, **96**, 045705.
39 M. E. Fleet, *Acta Crystallogr., Sect. B: Struct. Crystallogr. Cryst. Chem.*, 1981, **37**, 917.
40 W. C. Hamilton, *Phys. Rev.*, 1958, **110**, 1050.
41 H. Okudera, K. Kihara and T. Matsumoto, *Acta Crystallogr., Sect. B: Struct. Sci.*, 1996, **52**, 450.
42 S. Klotz, G. Steinle-Neumann, T. Strässle, J. Philippe, T. Hansen and M. J. Wenzel, *Phys. Rev. B*, 2008, **77**, 012411.
43 D. J. Huang, C. F. Chang, H.-T. Jeng, G. Y. Guo, H.-J. Lin, W. B. Wu, H. C. Ku, A. Fujimori, Y. Takahashi and C. T. Chen, *Phys. Rev. Lett.*, 2004, **93**, 077204.
44 C. T. Chen, Y. U. Idzerda, H.-J. Lin, N. V. Smith, G. Meigs, E. Chaban, G. H. Ho, E. Pellegrin and F. Sette, *Phys. Rev. Lett.*, 1995, **75**, 152.
45 J. H. van Vleck, *The Theory of Electric and Magnetic Susceptibilities*. London, Oxford University Press, 1966.